RSC Advances

COMMUNICATION

View Article Online
View Journal | View Issue

Cite this: *RSC Adv.*, 2016, **6**, 34955

Conduction band discontinuity and carrier multiplication at the $Mg_xZn_{1-x}O/Mg_yZn_{1-y}O$ interface

Xiuhua Xie,[a] Binghui Li,*[a] Zhenzhong Zhang,[a] Shuangpeng Wang[b] and Dezhen Shen*[a]

Received 1st February 2016
Accepted 30th March 2016

DOI: 10.1039/c6ra02919a

www.rsc.org/advances

Carrier multiplication is one process for improving the performance of deep ultraviolet (DUV) photodetectors. Conduction band discontinuity can make electrons obtain additional kinetic energy by potential energy (equal to ΔE_C) reducing, and then have sufficient energy to impact a lattice generating electron–hole pairs to increase the internal photocurrent. An active layer consisting of four-period graded bandgap MgZnO with a steep $Mg_xZn_{1-x}O/Mg_yZn_{1-y}O$ heterointerface, in which an impact ionization process takes place, has been demonstrated. The fabricated photodetector shows a DUV detection capability with a cutoff wavelength at ~280 nm. The peak responsivity at about 250 nm nonlinearly increases with the applied reverse bias.

Due to radiation hardness, minimum power usage, intrinsic visible blindness and light weight, deep ultraviolet (DUV) photodetectors based on wide band gap semiconductors (WBGs) such as AlGaN, β-Ga_2O_3, diamond, BN and MgZnO with response cutoff wavelengths shorter than 300 nm are attracting more and more attention.[1–5] Up to the present, a quantity of novel DUV photodetectors based on WBGs have been demonstrated.[6] One of the pivotal processes for improving the performance of these innovative WBGs based DUV photodetectors is photon-generated carrier gain.[7] In principle, the gain can be realized by converting the kinetic energy (greater than $3/2E_g$) of energetic carriers into additional carriers *via* multiplication.[8] However, in turn, the wide bandgap is the main limitation in impact ionization, because of larger carriers accelerating voltage or distance.[9] Therefore, it appears to be very important of motion controlling of energy carriers by energy band engineering. Specifically, compare with the other WBGs members, MgZnO alloys have the unique characteristics of band alignment, namely, larger tunable bandgap (ZnO 3.37 eV to MgO 7.8 eV) and larger ratio of conduction-band (CB) offset to valence-band (VB) offset ($\Delta E_C/\Delta E_V$) between different Mg content.[10–12] Motivated by the energy band characteristic of MgZnO, it is possible to rebuild an active layer tending to carriers impact ionization, *via* graded bandgap and steep heterointerface.

In this letter, we report a carrier multiplication layer consisted of four-period graded bandgap MgZnO. Since the larger CB discontinuity in the steep $Mg_xZn_{1-x}O/Mg_yZn_{1-y}O$ heterointerface, the electrons obtain additional kinetic energy by potential energy (equal to ΔE_C) reducing, and then have sufficient energy to impact lattice generating electron–hole pairs to increase internal photocurrent. The DUV photodetector, in this work, is a pn heterojunction type structure with a p-GaN as the hole conducting layer.

The heterostructure used in this work was grown with dual growth chamber MBE system (DCA Finland P600) equipped with radio-frequency O_2 plasma source 13.56 MHz for active O and solid-source effusion cells for Zn, Mg. Elemental Zn (7N grade), Mg (6N grade) and O_2 gas with 6N grade were used as molecular beam sources. All MgZnO content graded layers, with a ~30 nm-thick MgO buffer layer, were prepared on top of a 2 μm-thick p-GaN (0001) template grown by one of the chamber of MBE on 2 in. Unintentionally doped-GaN/c-sapphire substrate. The as-grown p-GaN (Hall-effect data, free holes concentration $\sim 5 \times 10^{17}$ cm^{-3} and mobility ~15 cm^2 V^{-1} s^{-1}) has been transferred from the nitrides chamber to the oxides sides by ultrahigh vacuum channel. The gradient of energy bandgap was produced by spatially varying the stoichiometry of Zn. In order to modulate the composition of ternary $Mg_xZn_{1-x}O$ alloy layers, two effusion cells for Zn are used. During growth, the background pressure was kept at 5×10^{-6} Torr depending on the Mg and Zn flux. The O_2 flow rate was 3.2 sccm, controlled by a leak valve. The radio-frequency excitation power was 290 W with a steady plasma brightness level. The growth temperature was 450 °C controlled by a thermocouple in the whole growth periods. A nude ionization gauge which working in front of the substrate, was adopted to measure the beam equivalent pressures (BPR) of Mg and Zn molecular beam. In this work, the BPR

[a]*State Key Laboratory of Luminescence and Applications, Changchun Institute of Optics, Fine Mechanics and Physics, Chinese Academy of Sciences, Changchun 130033, People's Republic of China*

[b]*The Institute of Applied Physics and Materials Engineering, University of Macau, Avenida da Universidade, Taipa, Macau, China*

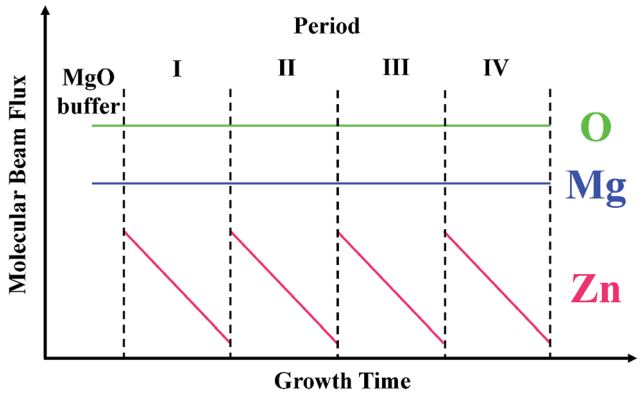

Fig. 1 Diagrams of Zn, Mg, and O molecular beam fluxes *vs.* growth time in period modulated growth schemes.

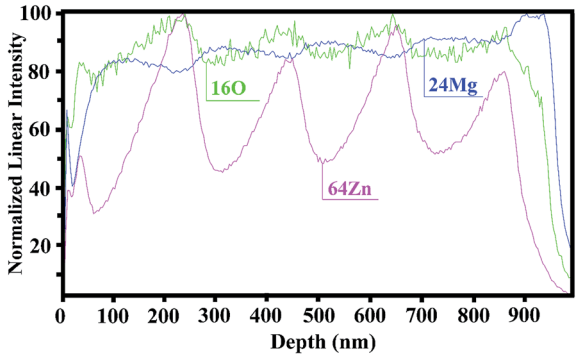

Fig. 2 The Mg, Zn, O depth profiles in linear intensity scale and after a 100% normalization for a better profile comparison.

of Mg was 7.2 × 10^{-8} Torr. Meanwhile, the BPR of Zn was decreasing from 3.5 × 10^{-7} to 4.6 × 10^{-8} Torr during each growth period. The growth time of each period is one hour. The growth process is illustrated in Fig. 1. In the precise control of effusion cell temperature ramp rate and shutter, the molecular beam flux for Zn was monotonically decreasing, during each graded layer growth period. The depth profiles of Mg, Zn, O atoms was investigated by secondary ion mass spectrometry (SIMS) measurements with cesium 133 (133Cs) as primary ion source. The reflectance spectrum of the four-period graded bandgap MgZnO layer measured at room temperature and determines the minimum bandgap, under normal incidence. For the device fabrication process, aluminium/indium (60/30 nm-thick) and nickel/gold (60/30 nm-thick), served as the electrodes, were deposited and patterned on MgZnO and p-GaN, respectively, using thermal evaporation and lift-off process. Part of MgZnO pattern was etched using 0.1% dilute hydrochloric acid with p-GaN surface exposed. Hall measurement system (Lakeshore HMS7707) was employed for current–voltage (*I–V*) characterization of the photodetector. The spectral response of the DUV photodetector was measured using a 150 W xenon lamp, an optical chopper (EG&G 192), a lock-in amplifier (EG&G 124A), and a monochromator, in a synchronous detection scheme. A UV-enhanced Si detector was employed to calibrate the system.

The SIMS depth profiles for the atoms Mg, Zn and O in graded bandgap layers are shown in Fig. 2 (linear scale after 100% normalization for a better profile comparison). The Mg, O profiles were maintained at a relative constant level through the layers. Simultaneously, the Zn profile corresponds to the intentional molecular beam flux precise controlling. There are four well-defined content graded layers, with four sharp interfaces, which indicating the larger ΔE_C achieved. These results suggest the kinetic energy of electrons probably surge by potential energy reducing (see discussion below).

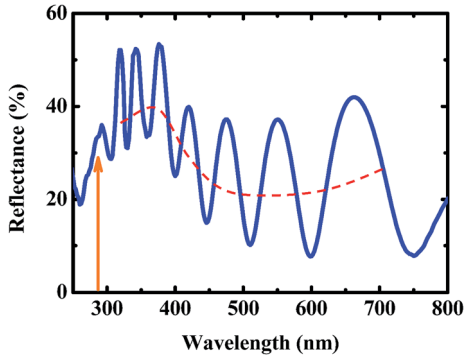

Fig. 3 The reflectance spectrum of four-period graded bandgap MgZnO. Narrowest optical bandgap marked with arrow.

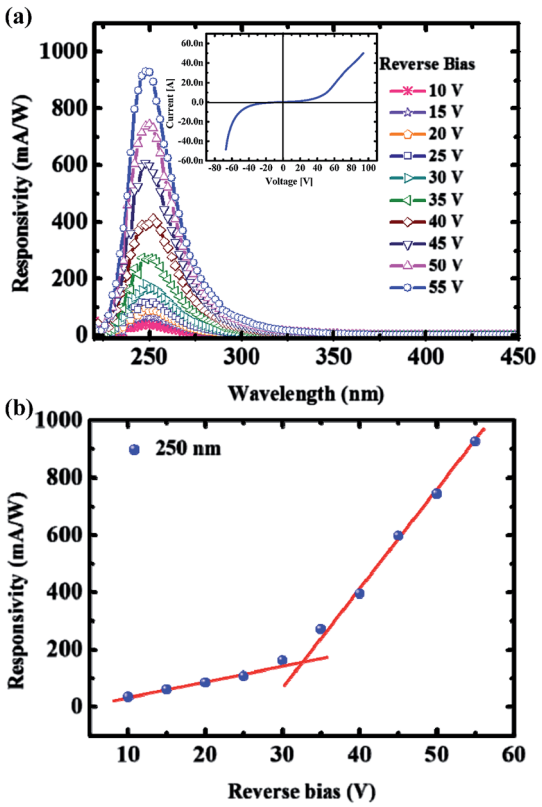

Fig. 4 (a) Spectral responsivity of the photodetector at different applied biases in normal incidence geometry. Inset shows the *I–V* characteristics of the device under dark, room temperature conditions. (b) Peak responsivity *vs.* reverse bias.

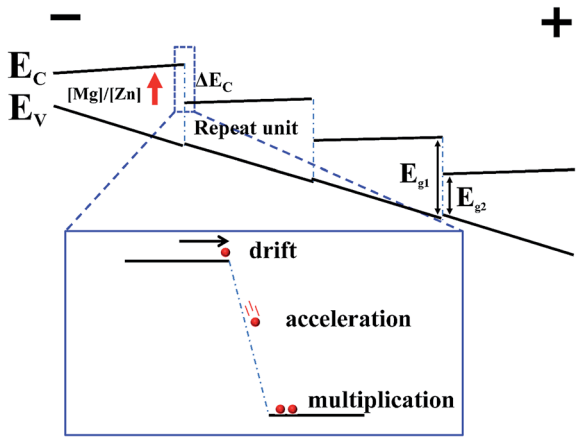

Fig. 5 Schematic representations of band alignment in four period graded bandgap MgZnO active layer, indicating the accelerated electron across the interface associated with impact ionization.

As can be seen in the Fig. 3, the graded bandgap MgZnO layers have a narrowest optical bandgap with dominated wavelength about 280 nm (arrow indicates the bandgap position). In the range of non-absorption, $\lambda > 280$ nm, reflectance spectrum clearly shows the interference which come from multiple reflection between the interfaces of MgZnO/GaN and air/MgZnO, besides, the effect of superposition (red dash line in Fig. 3) has been observed. It is interesting to note that the superposition of vibration indicates sufficient refractive index difference existed on the steep sides of $Mg_xZn_{1-x}O/Mg_yZn_{1-y}O$ interface. Additionally, the determination result of index difference is accordant to that of SIMS, the larger ΔE_C achieved.

Fig. 4(a) presents a series of spectral response of the photodetector at different applied biases in normal incidence geometry. The device shows a DUV detection capability with a cutoff wavelength at ~280 nm. There are no signal come from GaN side.[13] Intriguingly, it is found that the response spectra of all the reverse bias conditions only exhibit a single peak (~250 nm) shorter than the absorption edge of minimum bandgap of the graded layers, in strong contrast to the ordinary spectra observed in the other WBGs based photodetectors. This kind of performance is determined by spatial distribution of photon-absorption and photon-generated electrons (see discussion in below section). As shown in Fig. 4(b), the maximum responsivity at about 250 nm nonlinearly increases with the applied reverse bias. When the bias is greater than 35 V, the EQE is beyond 100% which indicates a large internal gain. Rather, the nonlinearity peak responsivity increase results from an extra gain due to an impact ionization process. And more notably, the bias voltage of ionization beginning is in consonance with *I–V* of the device, as can be seen from the inset of Fig. 4(a). Before breakdown, the saturation current show a gradually increasing trend. It indicates that there is multiplication mechanism present. Undoubtedly, the resulting gain is helpful for photon detection.

As can be seen from the $Mg_xZn_{1-x}O/Mg_yZn_{1-y}O$ energy band profile of the Anderson mode in Fig. 5, by spatially varying the stoichiometry of Zn, there are four graded bandgap MgZnO layers with steep heterointerface obtained. Due to the valence band maximum of MgO, ZnO dominated by anion 2p contributions,[14,15] during the Zn content decreasing, the raising of bandgap comes mainly from ΔE_C, which resulting a big potential energy difference at interface for electrons in conduction band. As opposed to the uniform content distribution in conventional active layer, the use of graded bandgap structure produces an extremely large field gradient towards interface. Two factors can account for photon-generated carriers multiplication in our DUV photodetector. First, as seen in Fig. 5, photon-generated electrons will be accelerated across the interface with additional kinetic energy obtained, suggesting a high probability of impact ionization. Second, another contribution to the ionization process could be the 'initial kinetic energy' effect in which electrons entering the heterointerface district have already acquired high energy. In our device, when the heterojunction is under suitable reverse bias, photo-generated electrons will traverse the interface of $Mg_xZn_{1-x}O/Mg_yZn_{1-y}O$ with eligible kinetic energy (bigger than $3/2E_{g2}$), equals to ΔE_C and initial kinetic energy, which will impact the lattice of MgZnO (E_{g2}) generating electron–hole pairs to increase internal photocurrent.

In summary, we reinvented a DUV photodetection active layer which electrons multiplication induced by larger conduction band discontinuity contribute to internal photocurrent increasing. The device showed peak responsivity at ~250 nm with high responsivity. The higher gain obtained by reverse bias raising is ascribed to the impact ionization process taking place in the content heterointerface with high initial kinetic energy of electrons.

Acknowledgements

We are grateful to CAMECA for their assistance with SIMS measurements. This work was supported by the National Natural Science Foundation of China (NSFC) under Grant No. 61376054 and 61505200.

Notes and references

1 E. Cicek, R. McClintock, C. Y. Cho, B. Rahnema and M. Razeghi, *Appl. Phys. Lett.*, 2013, **103**, 191108.
2 Y. B. Li, T. Tokizono, M. Y. Liao, M. A. Zhong, Y. Koide, I. Yamada and J. J. Delaunay, *Adv. Funct. Mater.*, 2010, **20**, 3972.
3 M. Y. Liao, Y. Koide and J. Alvarez, *Appl. Phys. Lett.*, 2007, **90**, 123507.
4 A. Soltani, H. A. Barkad, M. Mattalah, B. Benbakhti, J.-C. De Jaeger, Y. M. Chong, Y. S. Zou, W. J. Zhang, S. T. Lee, A. BenMoussa, B. Giordanengo and J.-F. Hochedez, *Appl. Phys. Lett.*, 2008, **92**, 053501.
5 X. H. Xie, Z. Z. Zhang, B. H. Li, S. P. Wang, M. M. Jiang, C. X. Shan, D. X. Zhao, H. Y. Chen and D. Z. Shen, *Opt. Express*, 2014, **22**, 246.
6 L. W. Sang, M. Y. Liao and M. Sumiya, *Sensors*, 2013, **13**, 10482.

7 R. Dahal, T. M. Al Tahtamouni, J. Y. Lin and H. X. Jiang, *Appl. Phys. Lett.*, 2007, **91**, 243503.
8 C. Bayram, J. L. Pau, R. McClintock, M. Razeghi, M. P. Ulmer and D. Silversmith, *Appl. Phys. Lett.*, 2008, **93**, 211107.
9 I. C. Kizilyalli, A. P. Edwards, H. Nie, D. Disney and D. Bour, *IEEE Trans. Electron Devices*, 2013, **60**, 3067.
10 X. Wang, K. Saito, T. Tanaka, M. Nishio, T. Nagaoka, M. Arita and Q. X. Guo, *Appl. Phys. Lett.*, 2015, **107**, 022111.
11 V. V. Solovyev, A. B. Van'kov, I. V. Kukushkin, J. Falson, D. Zhang, D. Maryenko, Y. Kozuka, A. Tsukazaki, J. H. Smet and M. Kawasaki, *Appl. Phys. Lett.*, 2015, **106**, 082102.
12 Y. F. Li, B. Yao, Y. M. Lu, B. H. Li, Y. Q. Gai, C. X. Cong, Z. Z. Zhang, D. X. Zhao, J. Y. Zhang, D. Z. Shen and X. W. Fan, *Appl. Phys. Lett.*, 2008, **92**, 192116.
13 X. H. Xie, Z. Z. Zhang, C. X. Shan, H. Y. Chen and D. Z. Shen, *Appl. Phys. Lett.*, 2012, **101**, 081104.
14 Y. Z. Zhu, G. D. Chen, H. G. Ye, A. Walsh, C. Y. Moon and S. H. Wei, *Phys. Rev. B: Condens. Matter Mater. Phys.*, 2008, **77**, 245209.
15 P. D. C. King, T. D. Veal, A. Schleife, J. Zuniga-Perez, B. Martel, P. H. Jefferson, F. Fuchs, V. Munoz-Sanjose, F. Bechstedt and C. F. McConville, *Phys. Rev. B: Condens. Matter Mater. Phys.*, 2009, **79**, 205205.